Available online at www.sciencedirect.com
SCIENCE DIRECT®

Journal of the European Ceramic Society 23 (2003) 1979–1986

www.elsevier.com/locate/jeurceramsoc

Electroconductive ceramic composites with low-to-zero shrinkage during sintering

M. Ade*, J. Haußelt

Institute for Microsystem Technology (IMTEK), Albert-Ludwigs-Universität Freiburg, Georges-Köhler-Allee 102, D-79110 Freiburg, Germany

Received 4 October 2002; accepted 11 November 2002

Abstract

Dense low or even zero shrinkage TiN/Si_3N_4 and ZrN/Si_3N_4 composites have been obtained by reaction of transition metal silicides $TiSi_2$, $ZrSi_2$ and Ti_5Si_3 with nitrogen gas in the temperature range 700–1500 °C. After transformation to nitrides, densification of the reaction-bonded composites is achieved (95–97% TD) in a subsequent sintering step up to 1800 °C in flowing nitrogen. Since the nitridation reaction is accompanied by volume expansions, linear shrinkage of the sinter bodies in relation to the die-pressed powder compacts is very low. In the case of $TiSi_2$ even zero shrinkage was achieved by adjusting the green density during axial compaction by variation of the applied stress. The electrical conductivities of the obtained ceramic specimen differ strongly due to the volume amounts of the conducting phases and different microstructures. The conductivity of the composites made from pure silicides or their mixtures ranges from 10^{-1} to 10^5 Ω^{-1} cm^{-1}.

Keywords: Composites; Reaction bonding; Silicides; Sintering; $TiN–Si_3N_4$; $ZrN–Si_3N_4$

1. Introduction

The outstanding properties of ceramics offer new applications in microsystem technology. In particular their chemical and thermal resistance make them suitable materials for microcomponents in chemical engineering. To make reactions at high temperature or under corrosive conditions feasible with microreaction technology, components manufactured entirely of ceramic have already been developed.[1,2] Alumina or zirconia are conventionally employed as ceramic materials, but also nitrides or carbides of transition metals are of special interest in this field, since they combine high thermal and chemical resistance with very good electroconductivities[3] (i.e. TiN: $\sigma_{20\ ^\circ C} = 4.6 \times 10^4\ \Omega^{-1}\ cm^{-1}$, ZrN: $\sigma_{20\ ^\circ C} = 7.4 \times 10^4\ \Omega^{-1}\ cm^{-1}$). The direct electric heatability of these materials overcomes many problems existing with external heating components of ceramic microparts. The electrical resistivity can be adjusted by using ceramic matrix composites of an electroconductive compound (TiN, TaN, TiC, ZrB_2, $MoSi_2$) and an insulating compound (Al_2O_3, Si_3N_4, SiC).[4–6]

The application of ceramic materials for microcomponents is often limited by the accuracy required of the micropatterned parts. Dimensional tolerances of 0.1% or less are hard to meet with conventional ceramic manufacturing processes, since the accuracy is strongly affected by the inevitable sintering shrinkage. Final machining, a cost-expensive but common process step in the manufacturing of big ceramic parts, is neither technically nor economically feasible for micropatterned components.

According to Greil[7] the manufacturing accuracy of a ceramic component shows a linear dependence to both sinter shrinkage and shrinkage tolerance. Shrinkage tolerance is strongly affected both by the appropriate shaping process in order to achieve a homogenous green density and the precise control of debinding and sintering. On the other hand, with appropriate near net shape forming processes and controlled thermal treatment,

* Corresponding author at present address: Institute for Inorganic and Analytical Chemistry, Albert-Ludwigs-Universität Freiburg, Albertstrasse 21, D-79104 Freiburg, Germany. Tel.: +49-761-203-6102; fax: +49-761-203-6012.
E-mail address: martin.ade@ac.uni-freiburg.de (M. Ade).

0955-2219/03/$ - see front matter © 2003 Elsevier Science Ltd. All rights reserved.
doi:10.1016/S0955-2219(02)00427-2

reduction of shrinkage is becoming the limiting factor with respect to the attainable accuracy.

Reduction of sinter shrinkage can be achieved by using a reaction-bonding process. Fig. 1 schematically compares length change during conventional sintering and a reaction-bonding process implying a volume expanding chemical reaction. A green body of a precursor material is subjected to a chemical reaction which leads to volume expansion and yields the desired ceramic material. The residual porosity in the reaction-bonded ceramic can be eliminated in a subsequent post-sintering step.

Following this scheme, low-to-zero shrinkage Al_2O_3 and mullite ceramics were produced by the reaction-bonded aluminium oxide process (RBAO).[8,9] Shrinkage-free $ZrSiO_4$ ceramics with densities up to 95%TD have been obtained by oxidation of compacts of $ZrSi_2$, ZrO_2 and polysiloxane as starting materials and subsequent sintering at 1600 °C.[10] For non-oxide ceramics besides the well known reaction-bonded silicon nitride (RBSN) and reaction-bonded silicon carbide (RBSC) processes, near net-shape manufacturing has been widely investigated by Greil and coworkers[11] in terms of the active filler controlled pyrolysis process (AFCOP).

The linear shrinkage S to be expected when a green ceramic body is converted into a dense ceramic body can be calculated by the following equation:[10]

$$S = \sqrt[3]{\left(1 + \sum_i \tilde{V}_i \cdot \Delta\tilde{V}_i\right)\frac{\tilde{\rho}_{\text{green}}}{\tilde{\rho}_{\text{sinter}}}} - 1 \qquad (1)$$

$\Delta\tilde{V}_i$: rel. volume change of component i (%)
$\tilde{V}_i$: rel. volume fraction of component i (%)
$\tilde{\rho}$: rel. densities of green, resp. sinter body (%TD).

The key to achieving low-to-zero shrinkage is to apply an appropriate precursor compound with a sufficiently high volume expansion $\Delta\tilde{V}$ during reaction-bonding. In this context transition metal silicides are interesting precursors since they can be converted into composites of transition metal nitrides—an electroconductive phase—and silicon nitride—an insulating phase by reaction with pure nitrogen gas [Eqs. (2)–(4)].

$$6\ TiSi_2 + 11\ N_2 \rightarrow 6\ TiN + 4\ Si_3N_4 \qquad (2)$$

$$6\ ZrSi_2 + 11\ N_2 \rightarrow 6\ ZrN + 4\ Si_3N_4 \qquad (3)$$

$$2\ Ti_5Si_3 + 9\ N_2 \rightarrow 10\ TiN + 2\ Si_3N_4 \qquad (4)$$

Table 1 lists characteristic data for the nitridation reactions of the three compounds. The relative volume expansions $\Delta\tilde{V}$ were calculated using X-ray densities from crystallographic data.[12] The volume amounts of the electroconductive transition metal nitrides $\tilde{V}_{\text{cond.}}$ in all three mixtures exceed the threshold of 16 vol.% for 3D-percolation of spheres assuming random packing and equal sphere sizes.[13] Thereby, in absence of an

Table 1
Calculated mass $\Delta\tilde{m}$ resp. volume changes $\Delta\tilde{V}$ of the investigated transition metal silicide precursor compounds during nitridation reactions and volume amount $\tilde{V}_{\text{cond.}}$ of electroconductive transition metal nitride in the resulting mixture

	$\Delta\tilde{m}$ (%)	$\Delta\tilde{V}$ (%)	$\tilde{V}_{\text{cond.}}$ (%)
$TiSi_2$	+49.3	+60.1	28.1
$ZrSi_2$	+34.8	+44.5	32.1
Ti_5Si_3	+38.7	+35.7	56.1

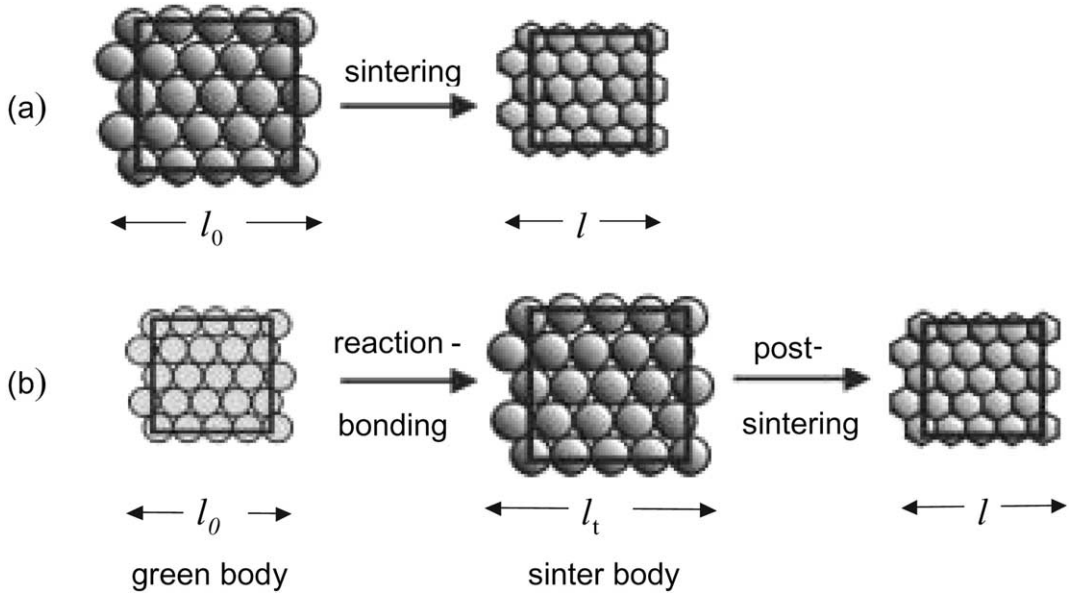

Fig. 1. Dimensional changes during manufacturing of ceramics by (a) conventional sintering, (b) reaction-bonding with volume expansion and subsequent post-sintering.

unfavourable array microstructure, all three composites should exhibit low electrical resistivities. According to the M/Si-ratio in the precursor compound the lowest resistivity should be expected for the composite based on Ti_5Si_3.

2. Experimental procedure

The starting silicide powders were $TiSi_2$ (Alfa Aesar, 99.5%, $d_{50}=10$ μm), $ZrSi_2$ (Alfa Aesar, 99.5%, 2–4% Hf, $d_{50}=10$ μm) and Ti_5Si_3 (Cerac Inc. 99.5%, $d_{50}=15$ μm). The powders were milled for 8 h in heptane (ball mill, ZrO_2-milling-bowl and -balls) to reduce the grain size to $d_{50}<2$ μm. After drying the powder was suspended in ethanol together with Al_2O_3 (Alcoa CT 3000 SG, 99.85%, $d_{50}=0.7$ μm) and Y_2O_3 (Alfa Aesar, 99.99%, $d_{50}<1$ μm) and polyvinylbutyral (PVB), which was added as a binder. Ethanol was removed under vacuum using a rotary evaporator. The composition of the granulates is listed in Table 2. In addition, mixtures of $TiSi_2$ and Ti_5Si_3 resp. $TiSi_2$ and $ZrSi_2$ with a volume ratio of 3:1 were prepared as granulates in the same manner.

Consolidation of the green bodies was achieved by axial pressing in the pressure range of 100–900 MPa and at pressing temperatures of 70–120 °C with steel dies of 10 mm diameter. Densities of the green bodies were calculated from weight and geometry of the cylindrical specimens.

Debinding and reaction-bonding of the green compacts and $TiSi_2$-powders were performed in a quartz-tube furnace (500–1000 °C) resp. in a graphite furnace for the high temperature range. For the nitridation reaction the specimen were placed in BN-crucibles and heated up to 1400–1550 °C with rates of 0.2–5 K/min. For the sintering step in the range 1500–1800 °C the specimens were placed in a protective bed of BN/Si_3N_4 with 20 wt.% sintering aids (Al_2O_3, Y_2O_3) and 2 wt.% SiO_2.

Processes occurring during the reaction-bonding were monitored by simultaneous thermal analysis (Netzsch STA 409) and dilatometry (Netzsch DIL 402C). The phase compositions were analysed by X-ray diffractometry (Siemens D5000) using CuK_α-radiation. Bulk densities were determined by the Archimedes method. Microstructural examinations of polished surfaces were performed by SEM (Zeiss DSM 960 equipped with a Link EDX system). Electrical resistivities were measured with the van der Pauw technique utilizing constant DC.

Table 2
Composition of granulates and powder properties

Granulate No.	Precursor compound	Volume ratio	d_{50}[a] (μm)	Al_2O_3 (vol.%)	Y_2O_3 (vol.%)	PVB (vol.%)
1	$TiSi_2$	–	1.6	3.2	6.6	10.0
2	$ZrSi_2$	–	0.9	4.4	5.2	10.0
3	Ti_5Si_3	–	3.3	3.4	6.9	10.0
4	$TiSi_2/Ti_5Si_3$	3:1		3.2	6.7	10.0
5	$TiSi_2/ZrSi_2$	3:1		2.9	5.4	10.0

[a] After milling.

3. Results and discussion

3.1. Fabrication of the green body

Although die pressing is not an appropriate shaping technique for micropatterned ceramics, it has some specific advantages for materials and process development in addition to easy handling. Since the shrinkage is

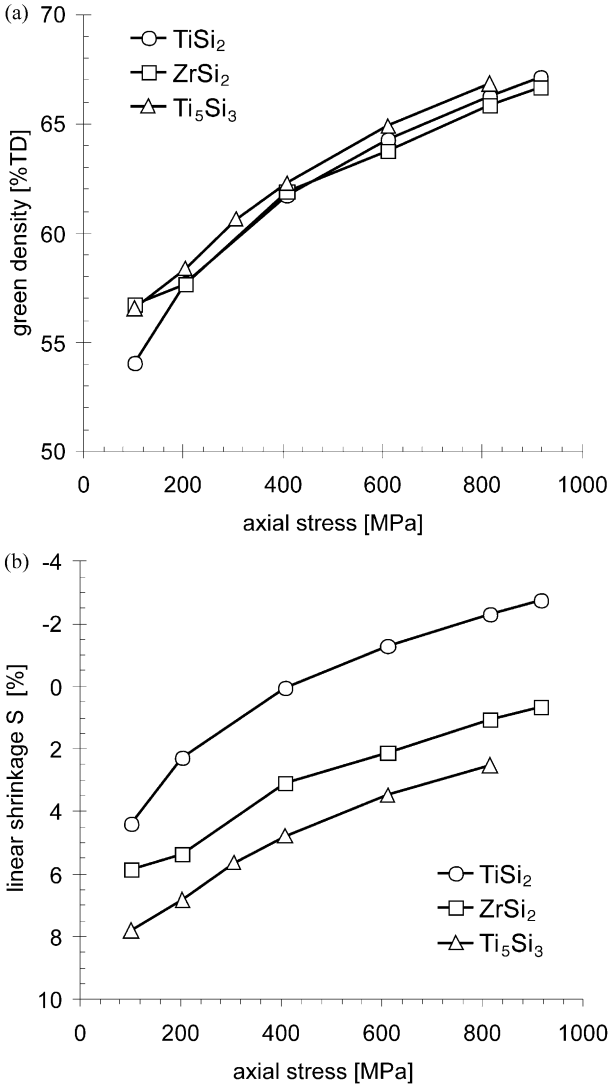

Fig. 2. (a) Compressibilities of silicide powder granulates with 10 vol.% PVB at 70 °C; (b) calculated linear shrinkage for an assumed relative sinter density of $\tilde{\rho}_{sinter}=95\%$TD.

related to the relative density of the green body [Eq. (1)] and since the green density of the compacted body depends on the applied pressure, the shrinkage can be easily adjusted by variation of the axial stress.

Fig. 2a shows the pressing curves at 120 °C, which are quite similar for all of the three investigated granulates. Relative densities of the green powder compacts (packing density of the powder particles) of $\tilde{\rho}_{green} = 58$–67%TD are obtained in the pressure range 200–600 MPa. It has to be emphasized that crack-free green bodies of 10 mm diameter and 3–5 mm sample height could be obtained up to 800 MPa at 70 °C. To prevent cracking also during reaction-bonding, an increase in pressing temperature to 120 °C has proved to be very effective.

Using Eq. (4) the expected linear shrinkage can be calculated from the measured green densities. The results are plotted in Fig. 2b in dependence of the applied axial stress at 70 °C pressing temperature. For example for a compaction pressure of 400 MPa the estimated linear shrinkage amounts to about 5% for Ti_5Si_3 and to 3.5% for $ZrSi_2$ while zero shrinkage should be expected for $TiSi_2$ as precursor compound. On the other hand it is obvious, that for the given powder characteristics and process parameters the required green densities for zero shrinkage of $ZrSi_2$ and Ti_5Si_3 derived ceramics lie well above the maximal axial pressure of 1000 MPa practically accessible with our laboratory equipment.

3.2. Reaction-bonding

As there are significant changes in mass and volume during reaction-bonding, the process can be well monitored by thermal gravimetric analysis and dilatometry. Fig. 3a shows the thermogravimetry traces of the three precursor compounds. For a better comparison the relative mass gains of the green specimens have been divided by the theoretical mass gains of granulates in order to obtain the "conversion" $c = \Delta\tilde{m}/\Delta\tilde{m}_{theo.}$ ($\Delta\tilde{m}_{theo.}$ from Table 1). Nitridation reaction of all three precursor compounds proceed in the temperature range 700–1450 °C and several steps of mass gain can be distinguished.

With Ti_5Si_3 as active component, specimens reach nearly 100% conversions at 1400 °C. On the other hand specimens with $TiSi_2$ res. $ZrSi_2$ only yield about 90% maximum conversion up to 1400 °C resp. 1500 °C and a "decrease of conversion" resulting from weight loss can be observed when rising the temperature still higher. As already shown for $TiSi_2$, both maximum degree of conversion and weight decrease at higher temperatures are strongly correlated to grain size and oxygen content of the precursor powder and the heating rate during thermal treatment.[14] The nitridation reaction of the precursor powders is obviously in competition with reactions between silicides or silicon and surface oxides (TiO_2, SiO_2, ZrO_2, $ZrSiO_4$) or with oxygen impurities in the furnace atmosphere yielding gaseous SiO, leading to a weight decrease of the sample.[15]

Fig. 3 shows dilatometry traces of green compacts of $TiSi_2$ (400 MPa), $ZrSi_2$ and Ti_5Si_3 (300 MPa) in flowing nitrogen. As can be clearly seen, the volume expansions during nitridation reactions are at least partially due to the linear expansions of the porous powder compacts. Assuming isotropic linear expansion of the powder particles in the compact during reaction-bonding, a maximum linear expansion Δl can be calculated from the volume amount of the active precursor compound A $\tilde{V}_A$ and the relative volume expansion $\Delta\tilde{V}_A$:

$$\Delta l = \sqrt[3]{1 + \Delta\tilde{V}_A \cdot \tilde{V}_A} \tag{5}$$

In Table 3 the calculated linear expansions of the experimentally observed expansions of the samples are compared with the calculated values. For Ti_5Si_3 there is a quite good coincidence of the values while for the nitridation of $TiSi_2$ and $ZrSi_2$ much lower expansions

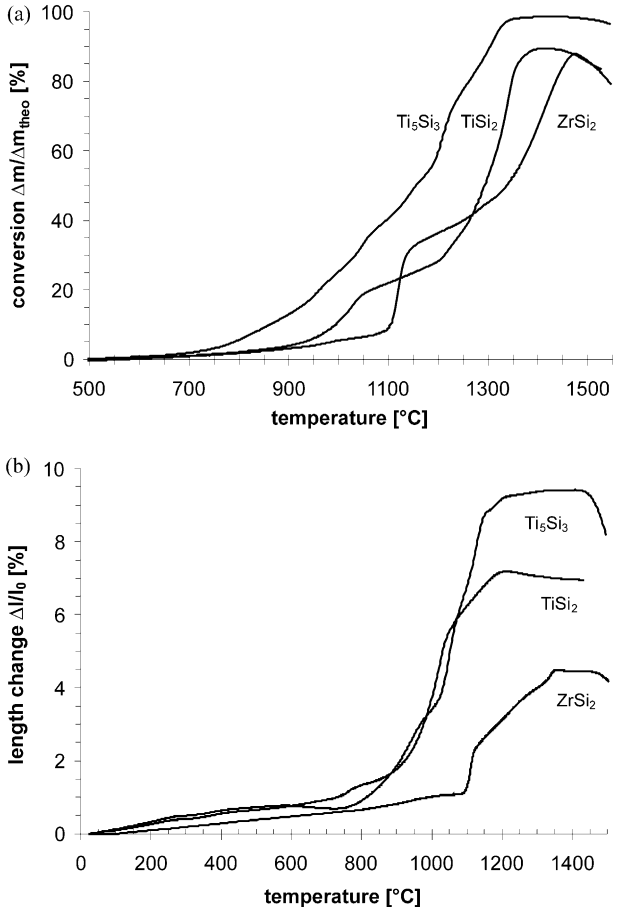

Fig. 3. (a) Conversion of the green compacts in nitrogen gas measured by thermal gravimetric analysis; (b) change of length of specimen determined by dilatometry. Specimens: green bodies with ∅ = 6 mm; heating-rate: 1 °C/min; gas flow: 100 ml/min N_2.

Table 3
Properties of specimen after compaction, reaction-bonding and post-sintering

Precursor	After compaction (green body)			Reaction-bonded (1450 °C)		Post-sintered (1750 °C/2 h)		Electrical resistivity (mΩcm)
	Axial stress	Temperature	$\tilde{\rho}_{green}$[a]	Linear expansion		Linear shrinkage S		
	(MPa)	(°C)	(%TD)	(Calcd.)[b] (%)	(Obs.)[c] (%)	(Calc.)[d] (%)	(Obs.)[e] (%)	
$TiSi_2$	400	70	61.7	15.4	6.2	0.0	2.3	2.9×10^{0}
$ZrSi_2$	400	70	61.4	11.8	3.5	3.7	4.2	0.9×10^{5}
Ti_5Si_3	300	120	62.1	9.6	8.5	5.2	6.8	1.5×10^{-1}

[a] Green density = packing density of powder particles.
[b] From Eq. (5).
[c] Observed maximal expansion from dilatometric trace (heating rate: 1 K/min); corrected for linear thermal expansion ($\alpha\sim7\times10^{-6}$ K^{-1}).
[d] Using Eq. (1) and a sinter density of 95%TD.
[e] Medium shrinkage calculated from exp. volume shrinkage of cylindrical specimen according Eq. (6).

are observed than calculated. This implies that only Ti_5Si_3 corresponds to the simple scheme of Fig. 1b, assuming isotropic expansion of the powder particles without a significant change in porosity. For the nitridation of $TiSi_2$ it has been shown that elemental silicon is formed as an intermediate product in the range 800–1100 °C.[14] Nitridation of silicon, as known from the reaction-bonded silicon nitride process (RBSN), proceeds without significant changes in volume, based on the specific reaction-mechanism.[16–18] This is in agreement with the observation that the maximum linear expansion in the dilatometric trace of $TiSi_2$ and Ti_5Si_3 is reached at temperatures approximately 100–150 °C lower than the maximum conversion in the thermogravimetric trace.

As was already mentioned for the weight change, the extent of length and volume change strongly depends on heating rates and holding times, but also on powder size and green density of the specimens. The decrease in length at 1450 °C for $TiSi_2$ and Ti_5Si_3 and at 1500 °C for $ZrSi_2$ indicates the beginning of the sintering process.

3.3. Post-sintering and shrinkage adjustment

After reaction bonding up to 1450 °C, the ceramics show densities in the range of 65–75%TD. Due to the high porosity the samples appear almost brownish and show high room temperature electrical resistivities ($\rho > 10^{1}$ Ωcm). In order to obtain ceramics with improved conductivities, densification has to be achieved by a post-sintering step. Since Si_3N_4 is the matrix phase of the resulting ceramic composite, pressureless sintering requires an appropriate sintering bed (BN/Si_3N_4). Fig. 4 shows the obtained relative sintering densities in dependence of the temperature for 2 h soaking time. Maximum relative densities of 95–97% are achieved at 1750 °C for all three ceramics. The relative mass $m/m_{theo.}$ of specimen shown the upper part of Fig. 4 indicates the amount of weight retained during thermal treatment with respect to the mass gain by nitrogen uptake during the nitridation reaction. The relative mass is mainly affected by gas evolution of SiO and Si_3N_4 during reaction-bonding resp. post-sintering. For pressureless sintering of Si_3N_4 with Al_2O_3 and Y_2O_3, intermixture of SiO_2 to a Si_3N_4/BN-powder bed has been reported to reduce weight loss[19] and improve the sinter behaviour.[20] Since significant mass losses occur beyond 1750 °C for composite ceramics obtained from $TiSi_2$ and $ZrSi_2$ a further increase in sintering temperature is detrimental to shrinkage reduction. As changes in weight and density are small in the temperature range 1700–1750 °C at 2 h soaking time, these conditions seems to be favourable to obtain a good reproducibility of manufacturing process.

According to the observed weight losses of the specimens after densification (2–6%), the linear shrinkage

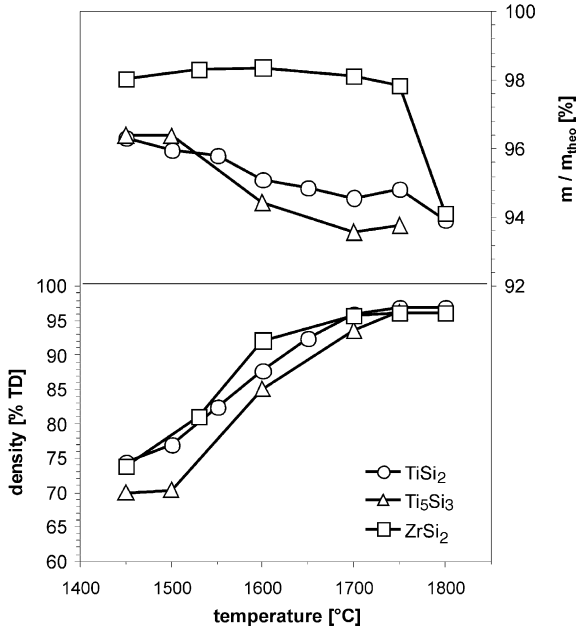

Fig. 4. Relative densities (lower part) and relative mass of ceramic specimens (upper part) during post-sintering in a BN/Si_3N_4 powder bed in dependence of the sintering temperature and 2 h annealing time.

observed is up to 2% higher than theoretically calculated, as can be seen from Table 3. In order to take the influence of various experimental parameters into account, an adjustment of shrinkage can be achieved by recording a calibration curve for a given granulate with definite composition and preparation procedure. Fig. 5 shows the shrinkage for TiN/Si_3N_4 ceramic composites emerging from $TiSi_2$ with respect to the green densities of the green bodies compacted at 120 °C after post-sintering at 1750 °C for 2 h soaking time.

As is obvious for the cylindrical specimens, change of sample height is different from change of sample diameter (Fig. 5). This is a well-known feature of axial pressure technique and is true for all the samples in this investigation. For easier interpretation a mean linear shrinkage $\bar{S}$ is calculated from the volume shrinkage ΔV:

$$\bar{S} = 1 - \sqrt[3]{1 + \Delta V} \quad (6)$$

Zero mean linear shrinkage—which is identical with zero volume shrinkage—is reached for a relative green density of about 64%TD. In accordance with the compressibility-curve of the $TiSi_2$ granulate at 120 °C a pressure of 480 MPa is required (see Fig. 2a).

3.4. Characterisation of the ceramics

The results of X-ray diffraction analysis on specimen post-sintered at 1750 °C for 2 h are shown in Fig. 6. TiN, ZrN and β-Si_3N_4 are the main crystalline phases. In the ceramic specimens emerging from $ZrSi_2$ a minor amount of an Y-containing α-SiAlON was detected, whereas the ceramic composites emerging from the titanium silicides contain minor amounts of the so-called H-Phase ($Y_5Si_3O_{12}N$ = N-apatite).

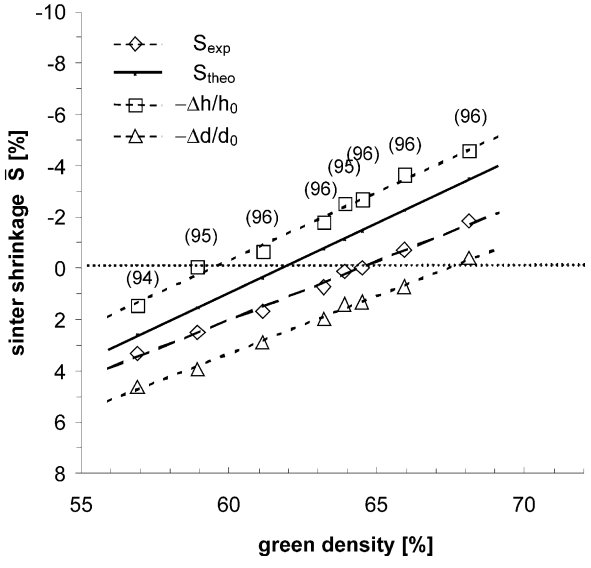

Fig. 5. Calibration curve for the adjustment of zero-shrinkage for composites emerging from $TiSi_2$. All specimen post-sintered at 1750 °C (2 h); numbers in brackets indicate the relative sinter density.

The microstructures of the three composites as revealed by SEM are shown in Fig. 7. The phases have been identified by EDX-analysis. The composite emerging from $TiSi_2$ shows a random structure of fine-grained TiN-particles (shown in light grey) in the silicon nitride matrix (dark grey). Corresponding to the higher volume content of titanium nitride in the ceramic that emerged from Ti_5Si_3, larger light areas can be observed. The few bright spots can be assigned to $Y_5Si_3O_{12}N$. In contrast to the TiN–Si_3N_4 composites the microstructure of the ZrN–Si_3N_4 composites exhibits an array structure. Agglomerates of ZrN of 2–5 μm size (white) are rather isolated by the surrounding Si_3N_4-matrix.

The electrical resistivities of the ceramic composites obtained from the different precursor compounds at 1750 °C are listed in Table 3 and are shown in Fig. 8. As expected, the TiN–Si_3N_4-composite made from Ti_5Si_3 shows the lowest resistivity of 0.15 mΩcm, a value about 7 times higher than for pure TiN (2.14×10^{-2} mΩcm). The composite emerging from $TiSi_2$ also shows a very low resistivity of around 3 mΩcm. Finally, the corresponding value of the ZrN–Si_3N_4 composites amounts to about 10^5 mΩcm, in agreement with the lack of percolation paths in the microstructure (see Fig. 7c). So in spite of very similar volume amounts of the conducting phases in the composites emerging from the MSi_2-compounds (see Table 1) their resistivities differ over five orders of magnitude due to the different microstructures developed during post-sintering.

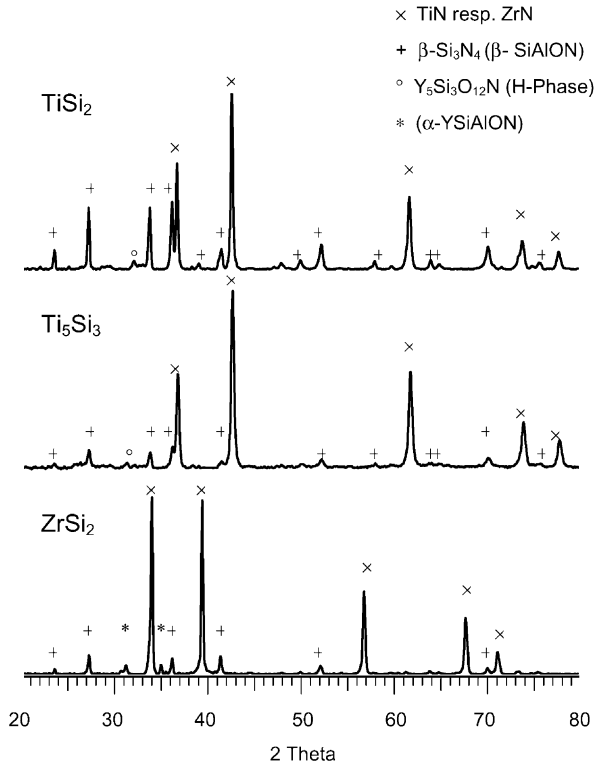

Fig. 6. X-ray diffraction analysis of reaction-bonded ceramics from transition metal silicides post-sintered at 1750 °C for 2 h.

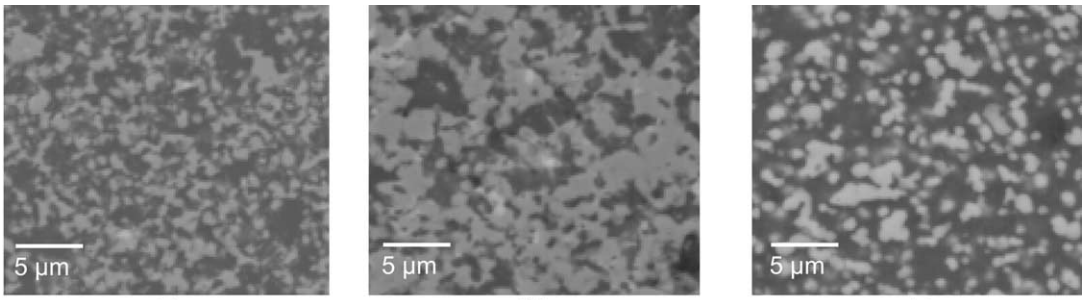

Fig. 7. Backscattered SEM images of the microstructures of reaction-bonded ceramic composites, post-sintered at 1750 °C for 2 h: (a) TiN/Si_3N_4 from $TiSi_2$, (b) TiN/Si_3N_4 from Ti_5Si_3, (c) ZrN/Si_3N_4 from $ZrSi_2$. Phase assignment by EDX-analysis: TiN resp. ZrN (light grey), Si_3N_4 (dark grey), $Y_5Si_3O_{12}N$ [bright spots in (a) and (b)].

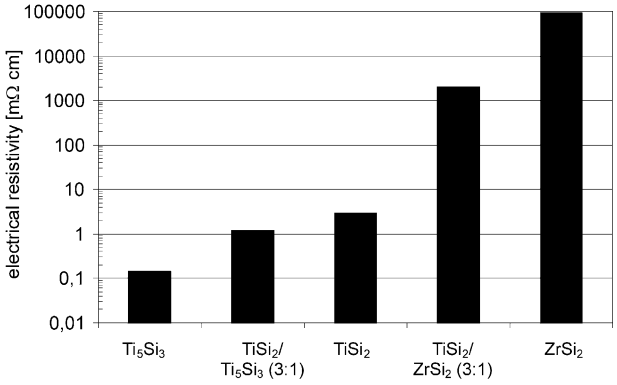

Fig. 8. Electrical resistivities at room-temperature of reaction-bonded composites made of the three types of precursors and mixtures thereof (volume ratios). Composites were post-sintered at 1750 °C for 2 h.

Fig. 8 also shows the electrical resistivities of the two composites manufactured from mixtures $TiSi_2/Ti_5Si_3$ and $TiSi_2/ZrSi_2$. As expected, the values of the mixed composites lie between those made from the single compounds and thus indicate the possibility of electroconductivity adjustment. Unfortunately, resistivity and shrinkage can not be altered independently over the whole range. But since even minor amounts of $ZrSi_2$ show strong influence on resistivity of the resulting ceramic composite, a shrinkage close to zero seems attainable in the resistivity range 10^0–10^4 mΩcm for green bodies with $TiSi_2$ as the main component. The required green densities (packing densities of powder particles) of $\tilde{\rho}_{green} = 63$–$67\%$TD can be realized with axial pressing at 400–600 MPa. Green densities in the same range should also be feasible by applying shaping techniques such as centrifugal casting[21] or hot molding[22] which are appropriate for manufacturing of micropatterned ceramic components.

4. Summary and conclusions

$TiN–Si_3N_4$ and $ZrN–Si_3N_4$ ceramic composites were obtained by nitridation of compacts of the three investigated silicides $TiSi_2$, Ti_5Si_3 and $ZrSi_2$ precursors with 90–98% yield for the reaction-bonding process. Relative densities of more than 95% were achieved by post-sintering the reaction-bonded specimens at 1750 °C in an appropriate sintering bed. The linear shrinkage during conversion of the green bodies—consolidated by axial pressing in the range 300–400 MPa—into dense sinter bodies amounts to 6–7% for $TiN–Si_3N_4$ ceramic composites emerging from Ti_5Si_3 and to 3–4% for $ZrN–Si_3N_4$ composites made from $ZrSi_2$. For $TiN–Si_3N_4$ ceramic composites obtained from $TiSi_2$ zero-shrinkage was achieved for 480 MPa and a pressing temperature of 120 °C. The electrical resistivities cover a range of six orders of magnitude (10^{-1}–10^5 mΩcm). Low-to-zero-shrinkage composites with adjusted electrical resistivities in the range 10^0–10^4 mΩcm seem to be achievable with axial pressing techniques using mixtures of $TiSi_2$, $ZrSi_2$ and Ti_5Si_3. The combination of appropriate shaping techniques for micropatterning with the developed reaction-bonding process should allow the low-to-zero shrinkage manufacturing of electroconductive ceramic microcomponents in the near future.

Acknowledgements

We are grateful to the Deutsche Forschungsgemeinschaft for financial support of this work.

References

1. Knitter, R., Bauer, W., Göhring, D. and Haußelt, J., Manufacturing of ceramic microcomponents by a rapid prototyping process chain. *Adv. Eng. Mat.*, 2001, **3**, 49–54.
2. Knitter, R., Göhring, D., Bram, M., Mechnich, P. and Broucek, R., In: *Topical Conference Proceedings, 4th Int. Conf. On Microreaction Technology*, AIChE Spring Meeting, Atlanta, Georgia, 5–9 March 2000, p. 455ff.
3. Wang, C. C., Akbar, S. A., Chen, W. and Patton, V. D., Electrical properties of high-temperature oxides, borides, carbides and nitrides. *J. Mater. Sci.*, 1995, **50**, 1627–1641.
4. Bellosi, A., Guicciardi, S. and Tampieri, A., Development and

characterization of electroconductive Si_3N_4–TiN composites. *J. Eur. Ceram. Soc.*, 1992, **9**, 83–93.
5. Winter, V., Entwicklung einer elektrisch heizbaren, mikrostrukturierbaren Keramik. PhD thesis, Karlsruhe, 1998.
6. Matsushita, Y., Nakamura, K. and Harada, K., *Electrically Conductive Sintered Ceramics and Ceramic Heaters*. US-Patent 4,555,358, 26 November 1985.
7. Greil, P., Near net shape manufacturing of ceramics. *Mat. Chem. Phys.*, 1999, **61**, 64–68.
8. Claussen, N. and Wu, S., Processing and properties of reaction-bonded Al_2O_3 (RBAO) and mullite ceramics. *Ceramic Trans.*, 1991, **22**, 631–646.
9. Holz, D., Pagel, S., Bowen, C., Wu, S. and Claussen, N., Fabrication of low-to-zero shrinkage reaction-bonded mullite composites. *J. Eur. Ceram. Soc.*, 1996, **16**, 255–260.
10. Hennige, V. D., Haußelt, J., Ritzhaupt-Kleissl, H.-J. and Windmann, T., Shrinkage-free $ZrSiO_4$-ceramics: characterisation and applications. *J. Eur. Ceram. Soc.*, 1999, **19**, 2901–2908.
11. Greil, P., Active-filler-controlled pyrolysis of preceramic polymers. *J. Am. Ceram. Soc.*, 1995, **78**, 835–848.
12. Villars, P., Calvert, L. D., ed., *Pearson's Handbook of Crystallographic Data for Intermetallic Phase* 1st edn. ASM, Metals Park, Ohio, 1985.
13. Zallen, R., *The Physics of Amorphous Solids*. John Wiley & Sons, New York, 1983.
14. Ade, M. and Haußelt, J., Materials and process development for the manufacture of shrinkage-free electroconductive ceramic composites. *Materials Week 2000 München* 25.-28.09, 2000.
15. Lin, W., Yang, J.-M., Ting, S.-J., Ezis, A. and Shih, C. J., Processing and microstructural development of *in situ* tin-reinforced silicon nitride/silicon oxynitride composites. *J. Am. Ceram. Soc.*, 1992, **75**, 2945–2952.
16. Moulson, A. J., Review—reaction-bonded silicon nitride: its formation and properties. *J. Mater. Sci.*, 1979, **14**, 1017–1051.
17. Jennings, H. M., Review—on reactions between silicon and nitrogen; part 1: mechanisms. *J. Mater. Sci.*, 1983, **18**, 951–967.
18. Ziegler, G., Heinrich, J. and Wötting, G., Relationship between processing, microstructure and properties of dense and reaction-bonded silicon nitride. *J. Mater. Sci.*, 1987, **22**, 3041–3086.
19. Hayashi, T., Munakata, H. and Suzuki, H., Pressureless sintering of Si_3N_4 with Y_2O_3 and Al_2O_3. *J. Mater. Sci.*, 1986, **21**, 3501–3508.
20. Lee, S.-H., Rixecker, G., Aldinger, F., Choi, S.-C. and Auh, K.-H., Effects of powder bed conditions on the liquid-phase sintering of Si_3N_4. *J. Mater. Res.*, 2002, **17**, 465–472.
21. Beylier, E., Pober, R. L. and Cima, M. J., Centrifugal casting of ceramic components. *Ceramic Trans.*, 1990, **12**, 529–536.
22. Alm, B. and Lenk, R., Formgebung von Mikrobauteilen und Mikrostrukturen aus Keramik. *Keram. Z.*, 2000, **52**, 312–315.